Four-dimensional ultrafast electron microscopy

Vladimir A. Lobastov, Ramesh Srinivasan, and Ahmed H. Zewail*

Laboratory for Molecular Sciences, Arthur Amos Noyes Laboratory of Chemical Physics, California Institute of Technology, Pasadena, CA 91125

Contributed by Ahmed H. Zewail, March 30, 2005

Electron microscopy is arguably the most powerful tool for spatial imaging of structures. As such, 2D and 3D microscopies provide static structures with subnanometer and increasingly with ångstrom-scale spatial resolution. Here we report the development of 4D ultrafast electron microscopy, whose capability imparts another dimension to imaging in general and to dynamics in particular. We demonstrate its versatility by recording images and diffraction patterns of crystalline and amorphous materials and images of biological cells. The electron packets, which were generated with femtosecond laser pulses, have a de Broglie wavelength of 0.0335 Å at 120 keV and have as low as one electron per pulse. With such few particles, doses of few electrons per square ångstrom, and ultrafast temporal duration, the long sought after but hitherto unrealized quest for ultrafast electron microscopy has been realized. Ultrafast electron microscopy should have an impact on all areas of microscopy, including biological imaging.

femtoscience | structural dynamics | ultrafast electron crystallography | ultrafast electron diffraction

When chemical and biological transformations involve complex transient structures with many possible conformations, one must address the nature of the 3D molecular structures, not only in their static state but also as a function of time, the fourth dimension. X-ray diffraction (refs. 1 and 2; see in particular the articles by L. Pauling, F. Crick, M. Perutz, and A. Rich in ref. 1) and NMR techniques (3, 4) have allowed the determination of 3D structures with atomic-scale resolution. Electron diffraction has similarly enabled structural determination, with the membrane protein structure of bacteriorhodopsin (5) being determined by using electron crystallography/microscopy (6). All these methods provide the equilibrium structure in crystals or the average structure in solution.

The motion of atoms in molecular structures occurs on the femtosecond time scale, and it is now possible to observe such coherent atomic motions in systems of various complexities, from the very small (two atoms) to the very large (e.g., proteins) (7). The mapping in time of dynamical trajectories unravels key features of the forces of motion and the associated effective and reduced energy landscape of structural dynamics. The complete structural determination at different times, however, requires the integration of space and time resolutions in 4D characterization of the structural change (8).

Transmission electron microscopy (TEM) with its wide-ranging arsenal of tools has long been a powerful method in many areas of research (9–20), allowing for subnanometer spatial resolution but lacking ultrashort time resolution. Optical microscopy, using fluorescent probes, e.g., green fluorescent proteins (21, 22), has provided the means to visualize dynamic events occurring *in vitro* and within cells. However, despite possessing the requisite temporal resolution, optical methods are limited in their spatial resolution to the wavelengths used, typically 200–800 nm. As pointed out by Mellman and Warren (23), the ultimate techniques would be those that have the spatial resolution of electron microscopy and the time resolution of optical methods. Many of the most important mechanistic questions can be answered if only we had "molecular video electron microscopy" (21). As mentioned above, the atomic length scale can be studied with x-ray and electron diffraction, but for biological and nanoscopic materials with characteristic length scales ranging from nanometers to micrometers, electron microscopy enjoys unique advantages.

It is the purpose of this paper to report the development of 4D ultrafast electron microscopy (UEM), which provides the ability to nondestructively image complex structures with the spatial resolution of TEM, but as snapshots captured with ultrafast electron packets derived from a train of femtosecond pulses. Here we present our first results of images and diffraction patterns obtained at 120 keV for materials (single crystals of gold, amorphous carbon, and polycrystalline aluminum) and for biological cells of rat intestines. The strobing packets contain on average one electron per pulse and the specimen dose is a few electrons per square ångstrom.

In our laboratory at Caltech, ultrafast electrons have been the probe of choice for studies in time-resolved diffraction for several reasons. The cross section for electron scattering is about six orders of magnitude larger than that for x-ray scattering, and the experiments are "table top" and can be implemented with ultrafast (femtosecond and picosecond) laser sources. Moreover, electrons are less damaging than x-rays to specimens per useful elastic scattering event, and they can be focused. Finally, with properly timed sequences of pulses, electrons can reveal transient structures of isolated molecules (refs. 24–27 and references cited in ref. 25), surfaces and adsorbates (28, 29), and thin crystals (30, 31). Unlike diffraction, imaging requires not only the generation of ultrashort electrons but much higher total number of electrons while preserving the time and spatial resolutions, contrast, and specimen dosage levels.

The conceptual design of UEM is shown in Fig. 1, which outlines the interfacing of the femtosecond optical system with the TEM. The laser system consists of a diode-pumped mode-locked Ti:sapphire laser oscillator, which generates sub-100-fs pulses at 800 nm with a repetition rate of 80 MHz and an average power of 1 W. Part of the beam can be used to heat or excite the sample and define the zero of time, while the rest is frequency doubled in a nonlinear crystal to yield 400-nm femtosecond pulses for generating the electron pulse train.

Space-charge broadening of electron pulses at the cathode surface and stability of the electron flux during imaging are two of the many technical issues we had to resolve. On a much longer time scale, high-speed electron microscopy (ref. 32 and references therein) has used single pulses of ≈20-ns duration and a current of 2 mA. Such pulses, which were used to study laser-induced melting in metals, pack within them large numbers of electrons that are, in fact, detrimental to achieving ultrashort pulses. Moreover, because the time window for imaging in those experiments is nanoseconds, the uncertainty in spatial resolution due to noise statistics is on the order of micrometers, as pointed out by Bostanjoglo (32).

To circumvent space-charge-induced broadening and the concomitant decrease in the ability of the microscope optics to focus these electrons, we have redesigned the TEM by directly illuminating the photocathode with extremely weak femtosecond pulses, but as a high-frequency train of pulses separated by 12.5

Abbreviations: UEM, ultrafast electron microscopy or microscope; TEM, transmission electron microscopy or microscope.

*To whom correspondence should be addressed. E-mail: zewail@caltech.edu.

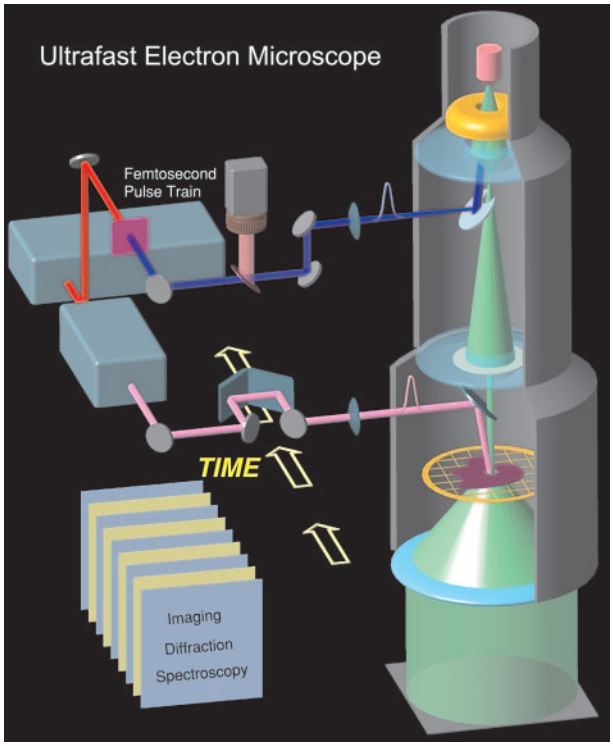

Fig. 1. The ultrafast electron microscope. Shown are the basic components, which involve interfacing the TEM with a train of femtosecond optical pulses to generate the on-axis electron beam in ultrafast packets of about one electron per pulse. The other optical beam delivers, after a well defined delay time, initiating pulses at the specimen, thus defining the zero of time. All other components, including the microscope lens system, charge-coupled device camera, and image processing, are described in the text.

ns (or longer). The pulse energy is ≈500 pJ, which, in concert with the present quantum efficiency of the electron extraction process at the photocathode surface, results in pulses along the microscope axis comprising on average one electron per packet. This crucial advance, generating electrons in a regime below the space-charge limit, whose trajectories can consequently be focused, empowered us to record images and diffraction patterns. In fact, our attempt to use amplified light pulses with much higher peak power density (on the order of 10^{12} W/cm^2) resulted in electron bunches that were impervious to focusing by the microscope optics, resulting no doubt in much broader pulses induced by electron–electron repulsion.

Materials and Methods

The basic microscope is a 120-kV G2 12 TWIN Tecnai TEM (FEI, Hillsboro, OR) modified for optical access with new entries, one toward the photocathode and another near the sample. The electron-generation assembly includes a MiniVogel Mount lanthanum hexaboride (LaB_6) cathode with a cone angle of 90° (Applied Physics Technologies, McMinnville, OR). The area of interaction was customized to be a flat 300 μm. The light pulses were carefully steered by using a computer-controlled mirror assembly and focused to ≈50 μm. In the conventional mode of operation, the cathode is heated and electrons are self-biased to create a virtual source below the aperture. However, the vastly decreased or nearly eliminated self-bias in our pulsed design positions the source right at the cathode surface, with its spatial extent being defined by the focused femtosecond pulses. The electron trajectories then follow the path defined by the lenses of the TEM, chiefly the condenser, the objective, and the projector lenses.

Single-electron detection was achieved through the use of an ultrahigh sensitive (UHS) phosphor scintillator, especially suitable for low-dose application, in conjunction with a charge-coupled device (CCD) camera (UltraScan 1000 UHS, Gatan, Pleasanton, CA). The digital camera is mounted on the microscope in an on-axis, below the chamber position. The 4-megapixel (Mpix) (2,048 × 2,048) chip has a pixel size of 14 × 14 μm with 16-bit digitization and a readout speed of 4 Mpix/s. To reduce noise, the CCD chip was thermoelectrically (Peltier) cooled to a temperature of about −25°C. The CCD images were recorded with the Digital Micrograph software, which runs embedded in the Tecnai user interface.

Cells were derived from the small intestine of a 4-day-old rat according to previously reported procedures (33), and the specimens were prepared by using standard TEM thin-section methods. The cells were positively stained with uranyl acetate, causing them to appear dark on a bright background. The specimens of amorphous carbon, polycrystalline aluminum, and single-crystal gold were TEM calibration materials (Ted Pella Inc., Redding, CA) mounted on microscope grids.

Results and Discussion

Fig. 2 shows the images obtained by using UEM for the so-called waffle-pattern diffraction grating replica with the line spacing being 463 nm. Images were obtained at various magnifications; here we display two of them. For calibration, we also show the observed background when the femtosecond pulses entering the microscope were blocked. The fact that no images were observed when the light pulses were blocked indicates that the electrons generated in the microscope were indeed those obtained optically and that thermal electrons were negligible. This finding is important because thermal electrons can be generated as a result of resistance heating and/or residual laser heating of the cathode. Detailed studies were conducted and will be reported elsewhere in a full account. The background was routinely checked for all images reported here. To compare the limits for resolution and contrast, we also display in Fig. 2 the images obtained in the TEM mode of the microscope. At these magnifications, the UEM and TEM images are of comparable quality. For higher magnifications up to ×110,000 we obtained UEM images of graphite on holey carbon grids (not shown). As before, there was no image in the background when the light pulses were shut off.

For atomic-scale investigations, we operated the UEM in the diffraction mode by adjusting the intermediate lens to select the back focal plane of the objective lens as its object. The results are shown in Fig. 3. The patterns were taken in pulsed and continuous modes for amorphous carbon, polycrystalline aluminum, and single-crystal gold. All these patterns can be indexed to give atomic plane spacings and symmetry of the unit cell.

Biological imaging is far more demanding, but the attributes of UEM encouraged us to test the viability of imaging biological cells. Fig. 4 shows the UEM images of rat intestinal cells at two different magnifications. These images, obtained with pulses of unprecedented time duration in exposure times of a few seconds, compare well with standard TEM images. Both the microvilli and the subcellular vesicles of these epithelial cells can be visualized in the UEM images.

The ultrafast time resolution of UEM has inimitable consequences. Because of the time scale, energy randomization is limited, residual healing is dissipative, and the atoms are nearly frozen in place (8), thus making feasible intact, single-particle, biomolecular and cellular imaging. Cryoelectron microscopy has emerged as a formidable method for studying the structure, assembly, and dynamics of macromolecules (34, 35), with time resolution limited to milliseconds as dictated by the freezing/mixing rates (36, 37). It should now be possible to freeze these structures in real time with UEM. Moreover, if biological or materials structural recovery is longer than the current pulse separation of 12.5 ns, it is relatively

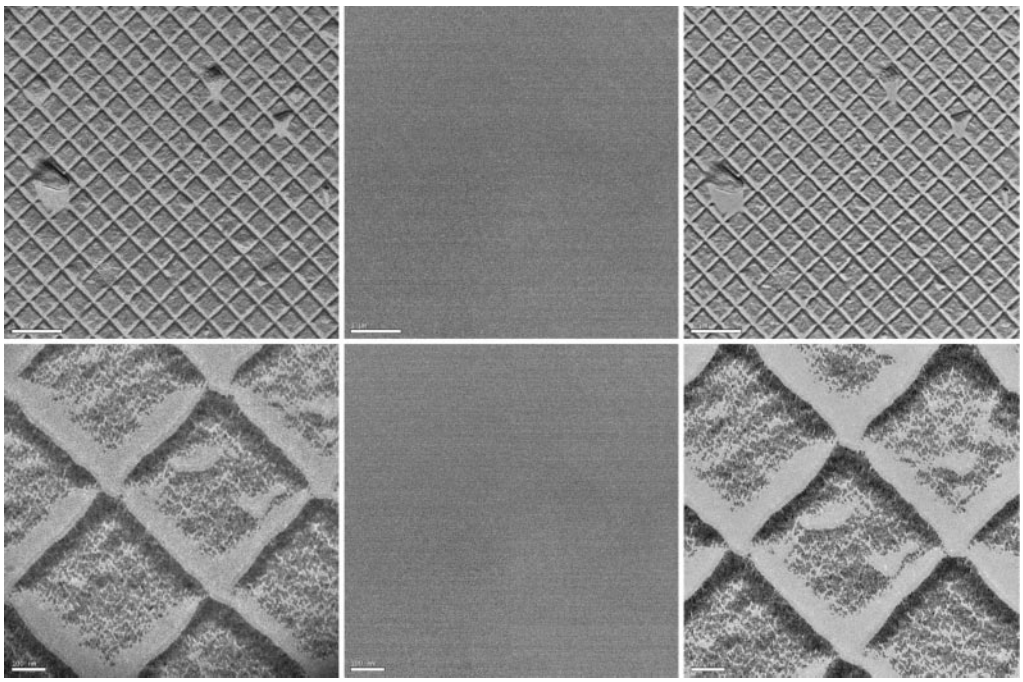

Fig. 2. UEM micrographs. The specimen (used for TEM magnification calibration) is a replica of 2,160 lines per mm waffle-pattern diffraction grating. (*Left*) UEM images obtained with ultrafast electron pulses. (*Center*) UEM background images obtained by blocking the photoelectron-extracting laser pulses. (*Right*) Images obtained in conventional TEM mode with continuous thermionic electrons. Images were obtained at many magnifications, two of which are shown here: ×3,200 (scale bar: 1 μm; *Upper*) and ×21,000 (scale bar: 100 nm; *Lower*). For carbon images (not shown), the magnification was ×110,000 (20-nm scale bar).

straightforward to select appropriately spaced pulses from the high-frequency train. The use of ultrafast pulsing at well defined temporal separations, when combined with the established methods of cryofixation, presents possibilities for limiting radiation damage of biological specimens.

Previous work from this laboratory (ref. 25 and references therein and ref. 28) has demonstrated subpicosecond electron pulses for 1,000 electrons per pulse at 30 keV. Electron pulses in UEM, with as few as one electron per pulse at 120 keV, now extend the time resolution to the femtosecond domain. The spatial reso-

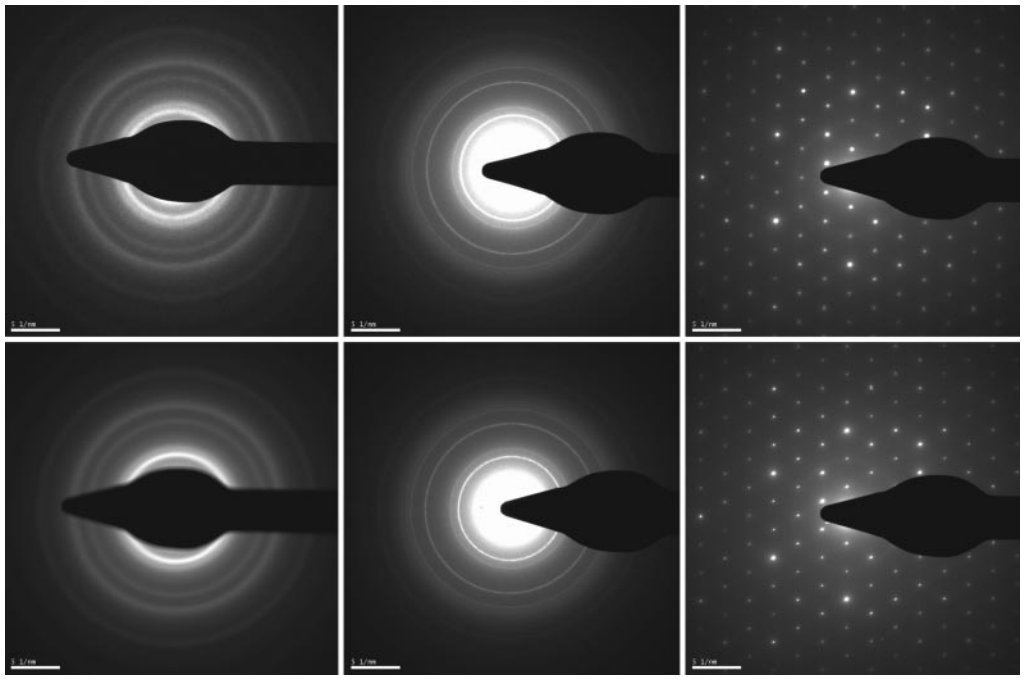

Fig. 3. UEM and TEM diffraction patterns for amorphous carbon (*Left*), polycrystalline aluminum (*Center*), and single-crystal gold (*Right*). (*Upper*) UEM diffraction patterns obtained with ultrafast electrons. (*Lower*) Patterns obtained in conventional TEM mode with continuous thermal electrons. The camera length for all diffraction patterns was 250 mm.

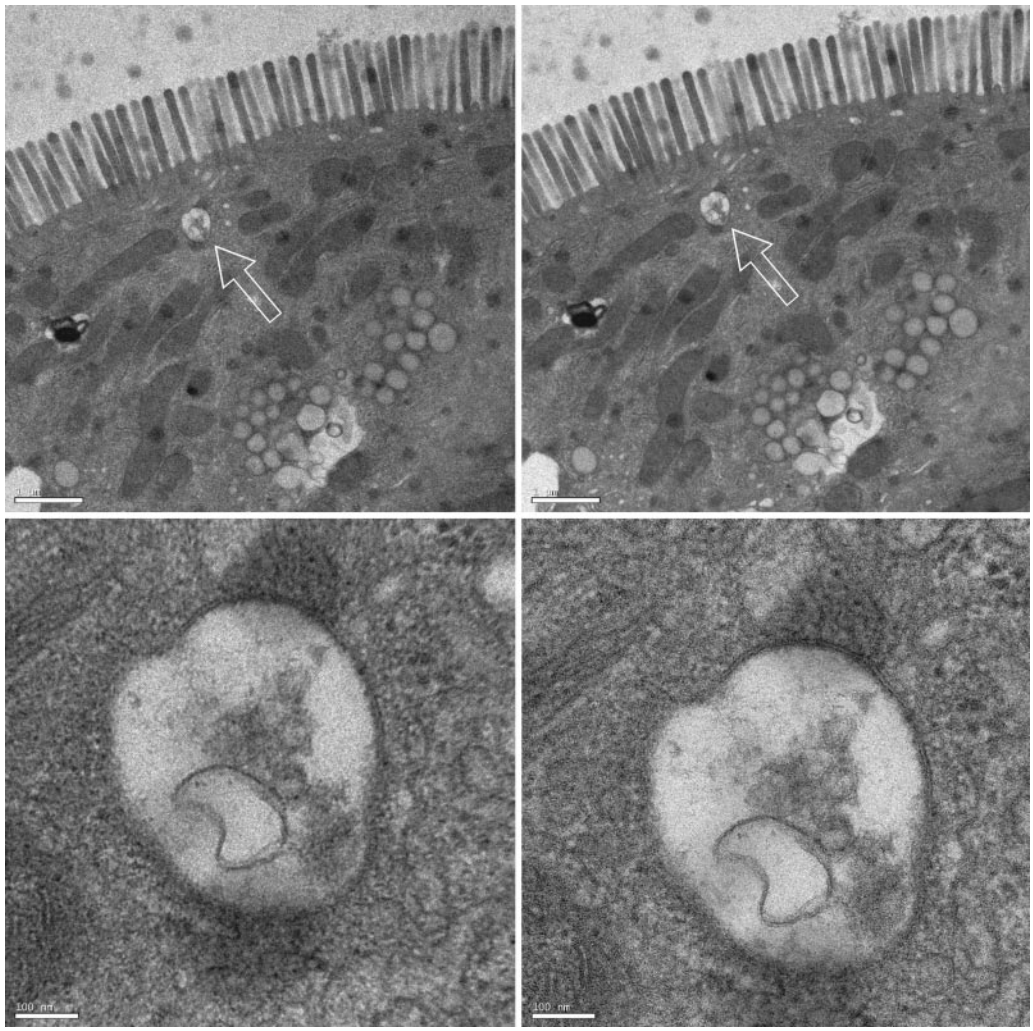

Fig. 4. UEM micrographs of positively stained rat intestinal cells. The images show the microvilli in the intestinal epithelium of the neonatal rat along with numerous small vesicles throughout the cytoplasm. (*Left*) UEM images at two magnifications (scale bars: 1 μm for *Upper* and 100 nm for *Lower*). (*Right*) Corresponding TEM images with the same exposure time (10 s). The arrows indicate the vesicle magnified in *Lower*.

lution can be further extended to the ångstrom (38) and even subångstrom realms (13, 39). Furthermore, as in the case of ultrafast electron diffraction and crystallography (24–31), UEM is now poised for measurements of structural dynamics. For such time-resolved investigations, the time axis is defined by distance steps in the arrangement of Fig. 1, noting that 1 μm of path difference corresponds to a frame separation of 3.3 fs, as routinely configured in our laboratories for diffraction and spectroscopic studies.

Concluding Remarks

It is perhaps worthwhile mentioning two concepts relevant to studies of structural dynamics by using UEM. First, there should be no concern about the uncertainty principle in limiting the atomic-scale resolution as we reach the femtosecond time scale. This is because the structures are prepared coherently, i.e., the ensemble of molecules follows a single-molecule trajectory (7, 40). Second, for any dynamical process, the change with time is continuous, and although some global events may occur at longer times, these events are triggered by local changes at early times. The primary events are an essential part of any complete description of the landscape and dynamics. Thus, even biological changes at longer times have their origin in the early atomic motions. It should be readily apparent that such dynamical evolution is critical to function. It does not escape our attention that UEM is a significant advance for this purpose.

4D UEM in real space and Fourier space encompasses spatial and temporal resolutions ranging from the atomic scale (ångstroms and femtoseconds) to the nanoscopic and microscopic domains. The microscope allows facile operation in two modes, the UEM mode and the conventional TEM mode, offering a universal methodology for structural studies in space and time. Moreover, because UEM has been designed to use femtosecond pulse trains from the oscillator alone, without the need for an ultrafast amplifier, it has the added technological advantage of being beguilingly simple and easy to integrate. Finally, with single-electron packets the resolution and focus in UEM are optimum. With these features of UEM, we foresee the emergence of new vistas in many fields, from materials science to nanoscience and biology.

A.H.Z. thanks Prof. David Tirrell for his encouragement and timely support of our vision. We acknowledge the genuine interest of Prof. Grant Jensen in the development of UEM and Dr. William Tivol for his generous assistance and stimulating discussions. We also thank Bill Anderson and Mike Stekelenburg of the FEI Company and Dr. Chuck Crawford of Kimball Physics, Inc., for invaluable discussions and assistance, and Dr. Wanzhong He for the biological specimen preparation. This work was supported by the National Science Foundation and the California Institute of Technology.

1. Zewail, A. H., ed. (1992) *The Chemical Bond: Structure and Dynamics* (Academic, San Diego).
2. Thomas, J. M. (1993) *Nature* **364,** 478–482.
3. Ernst, R. R. (1997) in *Nobel Lectures, Chemistry 1991–1995*, ed. Malmström, B. G. (World Scientific, Singapore), pp. 12–57.
4. Wüthrich, K. (2003) in *Les Prix Nobel: The Nobel Prizes* 2002, ed. Frängsmyr, T. (Almqvist & Wiksell, Stockholm), pp. 235–267.
5. Henderson, R. & Unwin, P. N. T. (1975) *Nature* **257,** 28–32.
6. Klug, A. (1992) in *Nobel Lectures, Chemistry 1981–1990*, ed. Malmström, B. G. (World Scientific, Singapore), pp. 77–109.
7. Zewail, A. H. (2000) in *Les Prix Nobel: The Nobel Prizes* 1999, ed. Frängsmyr, T. (Almqvist & Wiksell, Stockholm), pp. 274–367.
8. Zewail, A. H. (2005) *Philos. Trans. R. Soc. London A* **364,** 315–329.
9. Reimer, L. (1997) *Transmission Electron Microscopy: Physics of Image Formation and Microanalysis* (Springer, Berlin).
10. Thomas, J. M. & Terasaki, O. (2002) *Top. Catal.* **21,** 155–159.
11. Thomas, J. M. & Midgley, P. A. (2004) *Chem. Commun.*, 1253–1267.
12. Anderson, M. W., Ohsuna, T., Sakamoto, Y., Liu, Z., Carlsson, A. & Terasaki, O. (2004) *Chem. Commun.,* 907–916.
13. Spence, J. C. H. (1999) *Mater. Sci. Eng. Rep.* **26,** 1–49.
14. Howie, A. (2004) *Microsc. Microanal.* **10,** 685–690.
15. Baumeister, W. & Steven, A. C. (2000) *Trends Biochem. Sci.* **25,** 624–631.
16. Frank, J., Wagenknecht, T., McEwen, B. F., Marko, M., Hsieh, C.-E. & Mannella, C. A. (2002) *J. Struct. Biol.* **138,** 85–91.
17. Leapman, R. D. (2004) *Curr. Opin. Neurobiol.* **14,** 591–598.
18. Koster, A. J. & Klumperman, J. (2003) *Nat. Rev. Mol. Cell. Biol.* **4,** SS6-SS10.
19. Thomas, J. M., Terasaki, O., Gai, P. L., Zhou, W. Z. & Gonzalez-Calbet, J. (2001) *Acc. Chem. Res.* **34,** 583–594.
20. Thomas, J. M. & Gal, P. L. (2004) *Adv. Catal.* **48,** 171–227.
21. Tsien, R. Y. (2003) *Nat. Rev. Mol. Cell. Biol.* **4,** Suppl., SS16–SS21.
22. Gerlich, D. & Ellenberg, J. (2003) *Nat. Rev. Mol. Cell Biol.* **4,** Suppl., S14–S19.
23. Mellman, I. & Warren, G. (2000) *Cell* **100,** 99–112.
24. Srinivasan, R., Feenstra, J. S., Park, S. T., Xu, S. J. & Zewail, A. H. (2005) *Science* **307,** 558–563.
25. Srinivasan, R., Lobastov, V. A., Ruan, C.-Y. & Zewail, A. H. (2003) *Helv. Chim. Acta* **86**, 1761–1838.
26. Ihee, H., Lobastov, V. A., Gomez, U. M., Goodson, B. M., Srinivasan, R., Ruan, C.-Y. & Zewail, A. H. (2001) *Science* **291,** 458–462.
27. Williamson, J. C., Cao, J., Ihee, H., Frey, H. & Zewail, A. H. (1997) *Nature* **386,** 159–162.
28. Ruan, C.-Y., Vigliotti, F., Lobastov, V. A., Chen, S. & Zewail, A. H. (2004) *Proc. Natl. Acad. Sci. USA* **101,** 1123–1128.
29. Ruan, C.-Y., Lobastov, V. A., Vigliotti, F., Chen, S. & Zewail, A. H. (2004) *Science* **304,** 80–84.
30. Vigliotti, F., Chen, S., Ruan, C.-Y., Lobastov, V. A. & Zewail, A. H. (2004) *Angew. Chem. Int. Ed.* **43,** 2705–2709.
31. Thomas, J. M. (2004) *Angew. Chem. Int. Ed.* **43,** 2606–2610.
32. Bostanjoglo, O. (2002) *Adv. Imaging Electron Phys.* **121,** 1–51.
33. Abrahamson, D. R. & Rodewald, R. (1981) *J. Cell Biol.* **91,** 270–280.
34. Frank, J. (2002) *Annu. Rev. Biophys. Biomol. Struct.* **31,** 303–319.
35. Baumeister, W. (2005) *FEBS Lett.* **579,** 933–937.
36. Heymann, J. B., Conway, J. F. & Steven, A. C. (2004) *J. Struct. Biol.* **147,** 291–301.
37. Frank, J. (2001) *Methods* **25,** 309–315.
38. Haider, M., Uhlemann, S., Schwan, E., Rose, H., Kabius, B. & Urban, K. (1998) *Nature* **392,** 768–769.
39. Nellist, P. D., Chisholm, M. F., Dellby, N., Krivanek, O. L., Murfitt, M. F., Szilagyi, Z. S., Lupini, A. R., Borisevich, A., Sides, W. H. & Pennycook, S. J. (2004) *Science* **305,** 1741.
40. Zewail, A. H. (2001) *Nature* **412,** 279.